J Appl Electrochem (2008) 38:713–719
DOI 10.1007/s10800-008-9499-1

ORIGINAL PAPER

Electrodeposition of cobalt based ferro-magnetic metal nanowires in polycarbonate films with cylindrical nanochannels fabricated by heavy-ion-track etching

T. Ohgai · K. Hjort · R. Spohr · R. Neumann

Received: 27 July 2007 / Revised: 24 January 2008 / Accepted: 24 January 2008 / Published online: 5 February 2008

Abstract Polycarbonate films of thickness 30 μm were irradiated with heavy ions by applying a flux of 10^8 ions cm^{-2} to produce straight tracks perpendicular to the film surface. The tracks were preferentially etched in 6 M aqueous solution of sodium hydroxide to prepare cylindrical nanochannels. The channel diameters were tuned between 200 and 600 nm by varying the etching time. $Co_{81}Cu_{19}$ alloy nanowires were electrodeposited potentiostatically, while Co/Cu multilayered nanowires, consisting of alternating Co and Cu layers with thickness 10 nm, were synthesized by means of a pulse plating technique in channels of length 30 μm and diameter 200 nm. $Co_{81}Cu_{19}$ alloy nanowires showed an anisotropic magnetoresistance effect of 0.6%, and the giant magnetoresistance of Co/Cu multilayered nanowires reached up to 8.0%.

Keywords Heavy ion · Polycarbonate · Electrodeposition · Cobalt · Copper · Nanochannel

T. Ohgai (✉) · R. Spohr · R. Neumann
Gesellschaft für Schwerionenforschung (GSI), 64291 Darmstadt, Germany
e-mail: ohgai@nagasaki-u.ac.jp

T. Ohgai
Faculty of Engineering, Nagasaki University, Nagasaki 852-8521, Japan

K. Hjort
The Ångström Laboratory, Uppsala University, Box 534, 75121 Uppsala, Sweden

1 Introduction

Nanosized materials such as nanotubes, nanowires, and nanoparticles show novel physical and chemical properties on the basis of finite-size and quantum-effects. Among nanosized materials, nanowires are promising candidates as pioneering electron transport materials, applicable to magnetoresistive and optoelectronic devices in ultra-large-scale integration (ULSI). Nanowires can be grown by electrodeposition from aqueous solution into nanochannel templates [1–3] such as commercially available polycarbonate membranes [4–6] or anodized porous alumina membranes [7–11]. In commercial polycarbonate membranes, the nanochannels are distributed at random. Similarly, the angles between the channel axis and the film normal vary up to more than 10–20°. The shape of these nanochannels is also far from an ideal cylinder. In anodized aluminium oxide films, inter-channel distance is less than the channel diameter and typically below 100 nm. This makes lithography very difficult when only a few wires are to be coupled in a magnetoresistive device to give it high enough resistance and hence enhance its applicability. Furthermore, the oxide film is chemically unstable, e.g. dissolvable in acidic or alkaline aqueous solutions. Template synthesis techniques using nanochannel polymer films can be applied to fabricate nanosized electronic devices in ULSI. To realize the integration of this technique and microelectronics in ULSI, the size parameters such as channel length, channel diameter, and inter-channel distance must be controlled over a wide range. Lithographic galvanoforming (LIGA) using energetic heavy-ion beams can be applied to the polymer template synthesis. Using a modified heavy-ion LIGA technique, we have reported the fabrication of homogeneous Ni and Co nanowires with a wide range of aspect ratios in polycarbonate and polyimide films [12].

In a recent study Co/Cu nanowires grown in porous alumina membranes have shown high giant magneto resistance (GMR) values [11]. In this study, to ease the production of magnetoresistive devices of high resistance, we aim at synthesizing Co/Cu wires in a polymer template employing the modified heavy-ion LIGA technique. Here a polycarbonate film was irradiated with energetic heavy ions [13–18] to produce straight tracks (10^8 ions cm^{-2}), and subsequently the film was preferentially etched attacking the tracks to realize cylindrical nanochannels with an aspect ratio larger than 100. $Co_{81}Cu_{19}$ alloy nanowires and Co/Cu multilayered nanowires were electrodeposited in the template with channels of length 30 μm and diameter 200 nm. The anisotropic magneto resistance (AMR) effect of $Co_{81}Cu_{19}$ alloy nanowires as well as the GMR effect of Co/Cu multilayered nanowires was investigated.

2 Experimental

Figure 1 illustrates the fabrication process of Co/Cu multilayered nanowires electrodeposited in nanochannels obtained by the heavy-ion-track etching technique applied in this study: (a) recording of heavy-ion tracks, (b) etching of tracks, (c) formation of electrodes, (d) electrodeposition of Co/Cu nanowires. Polycarbonate films with a thickness of 30 μm were used as templates. First, by irradiating the sample with an ion beam from the UNILAC linear accelerator (GSI, Darmstadt, Germany), straight ion tracks with a density of 10^8 tracks cm^{-2} were created perpendicular to the film surface as shown in Fig. 1a. The tracks were selectively etched in a 6-M aqueous solution of NaOH to produce cylindrical nanochannels as depicted in Fig. 1b. The etching process following the irradiation was optimized to produce a uniform cross-section all along the channel with very small roughness. A copper layer of thickness 1 μm, which acts as cathode for the nanowire growth, was electrodeposited on a gold layer of thickness 100 nm sputtered on the membrane as shown in Fig. 1c. An aqueous electrolytic solution was synthesized from $CoSO_4 \cdot 7H_2O$ 120 g L^{-1}, $CuSO_4 \cdot 5H_2O$ 1.6 g L^{-1}, and H_3BO_3 45 g L^{-1} for electrodeposition of Co–Cu alloy nanowires and Co/Cu multilayered nanowires. A cathodic polarization curve was measured over a wide range of cathode potential to determine the optimum potential for Cu and Co deposition. Growth rates of nanowires were estimated by the channel-filling time, which was determined from the time-dependence of deposition current at each potential. Co/Cu multilayered nanowires were electrodeposited by alternately changing the cathode potential from −0.3 V vs. Ag/AgCl (for Cu layer) to −1.0 V (for Co layer) as shown in Fig. 1d. To determine the alloy composition of the wires, a sample was prepared as

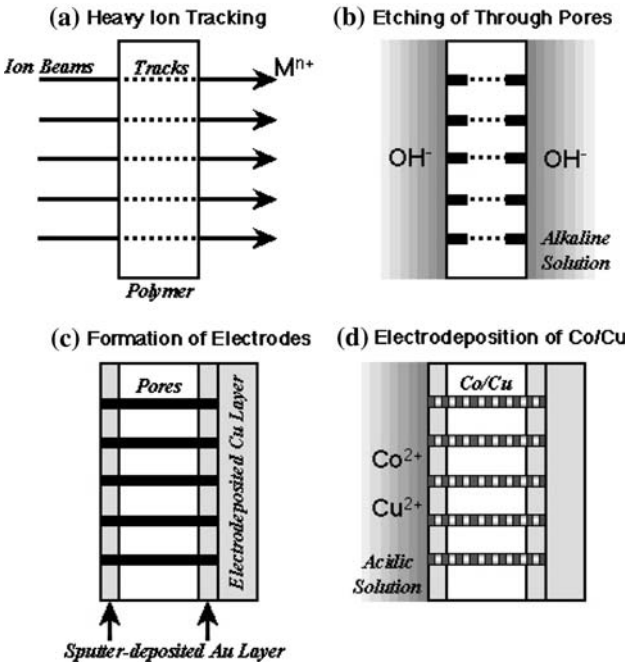

Fig. 1 Schematic of fabrication process of Co/Cu multilayered nanowires electrodeposited in nanochannels obtained by heavy-ion-track etching: (**a**) preparing latent tracks using heavy-ion beams, (**b**) etching of latent tracks leading to channels, (**c**) sputtering a gold layer on both sides of the surface and electrodeposition of Cu layer on the sputtered gold layer, (**d**) electrodeposition of Co/Cu nanowires in the channels

follows. First, nanowires were electrodeposited at constant cathode potential in polycarbonate channels with length 30 μm and diameter 200 nm. Then, the polycarbonate was dissolved in an organic solvent to expose the wires. Finally, the wire composition was determined by EDX. Co–Cu alloy nanowires electrodeposited at −1.0 V contained 81%-Co and 19%-Cu. To measure the wire resistance the wires were in situ contacted with a gold layer during the electrodeposition process as illustrated in Fig. 1d. Magnetoresistance curves were measured at room temperature applying a direct current of 10 μA and changing the magnetic field up to 10 kOe.

3 Results and discussion

3.1 Fabrication of nanochannels

Figure 2 shows the effect of film thickness on the monitoring current during etching of the heavy-ion tracks in polycarbonate films with thicknesses 10, 30, and 60 μm. During etching, a constant voltage (1 V) was applied between two gold electrodes separated by the membrane in 6 M aqueous NaOH. The time-dependence of the resulting current between the electrodes is displayed in Fig. 2. At the

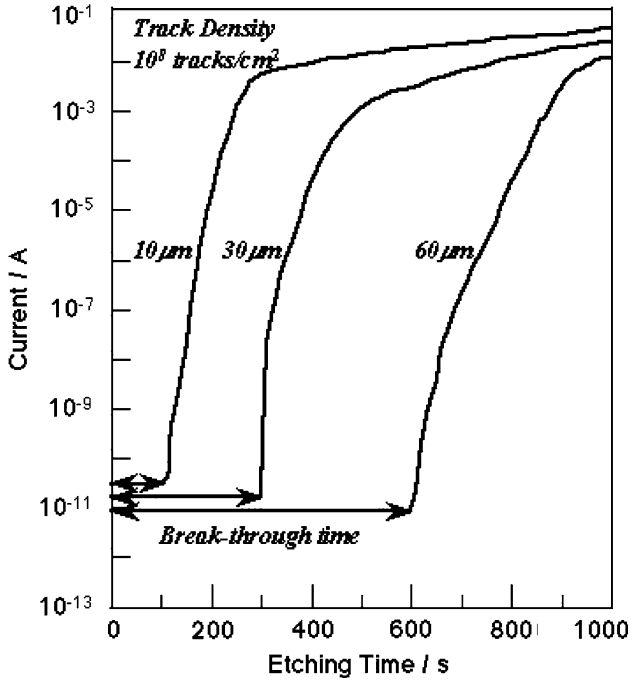

Fig. 2 Effect of film thickness on measured current during etching process in 6 M aqueous solution of NaOH at 323 K. The film thicknesses were 10, 30, and 60 μm

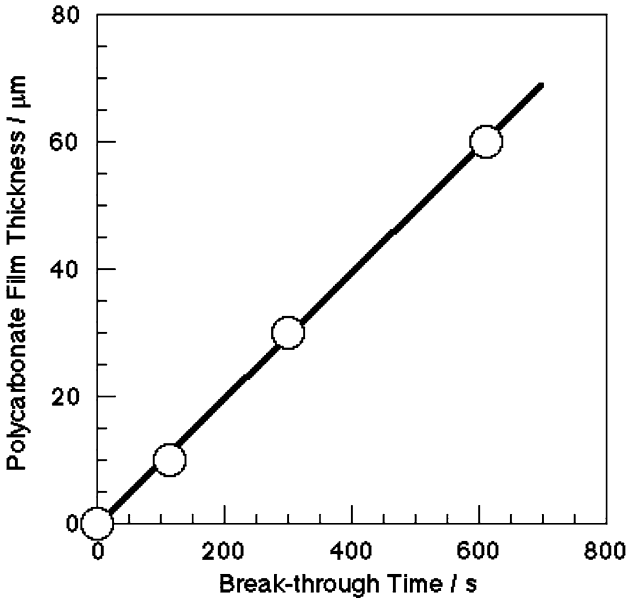

Fig. 3 Relationship between polycarbonate film thickness and break-through time for preparing channels in 6 M aqueous solution of NaOH at a temperature of 323 K

beginning of the etching, a very small current of the order of 10^{-11} A was observed, corresponding to a huge resistance (10^{11} Ω) measured between the electrodes. This resistance is due to the still unetched polycarbonate. The current increases drastically at an etching time of about 300 s when using the polycarbonate film with thickness 30 μm. At this break-through time, the channels reach the perforated state. After break-through, the current increases up to roughly 10^{-2} A, and a small resistance (10^{2} Ω) is measured between the electrodes. Figure 3 represents the relationship between polycarbonate film thickness and break-through time. As shown in this figure, with increasing film thickness, the break-through time also increases and the etching rate is estimated to be around 50 nm s^{-1}. Apel et al. reported etching rates of the order of 20 and 50 nm s^{-1} for single ion tracks in semicrystalline polycarbonate film with thickness 10 and 30 μm, respectively [19]. Chtanko et al. also reported that the etching rate of single ion tracks in semicrystalline polycarbonate film with thickness 20 μm was circa 50 nm s^{-1} [20]. The result obtained in this study corresponds well to the data reported in [19, 20].

Figure 4a–d display SEM images of etched nanochannels in polycarbonate films with thickness 30 μm obtained at etching times of 1,000, 1,500, 2,000, and 3,000 s, respectively. Each sample was sputter-coated with a thin gold layer to avoid electro-charging effects during SEM observation. The channel diameter increases with increasing etching time

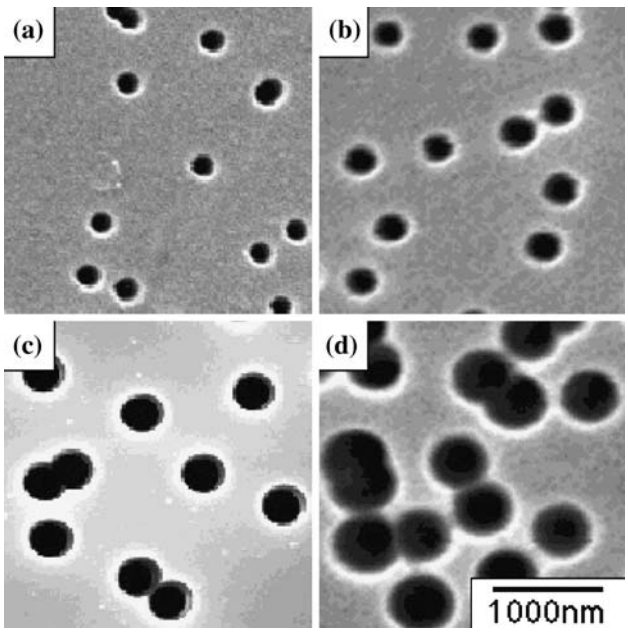

Fig. 4 SEM images of etched nanochannels in polycarbonate films with thickness 30 μm obtained at etching time 1,000, 1,500, 2,000, and 3,000 s for (**a–d**), respectively

and the distribution of the channel diameters is quite narrow. Figure 5 shows the time-dependence of channel diameter (a), channel cross-sectional area (b), and current (c) measured during track etching in the polycarbonate film with thickness 30 μm. As a function of etching time, the channel diameter increases as shown in Fig. 5a. The diameter can be tuned between 200 and 600 nm by varying the etching time.

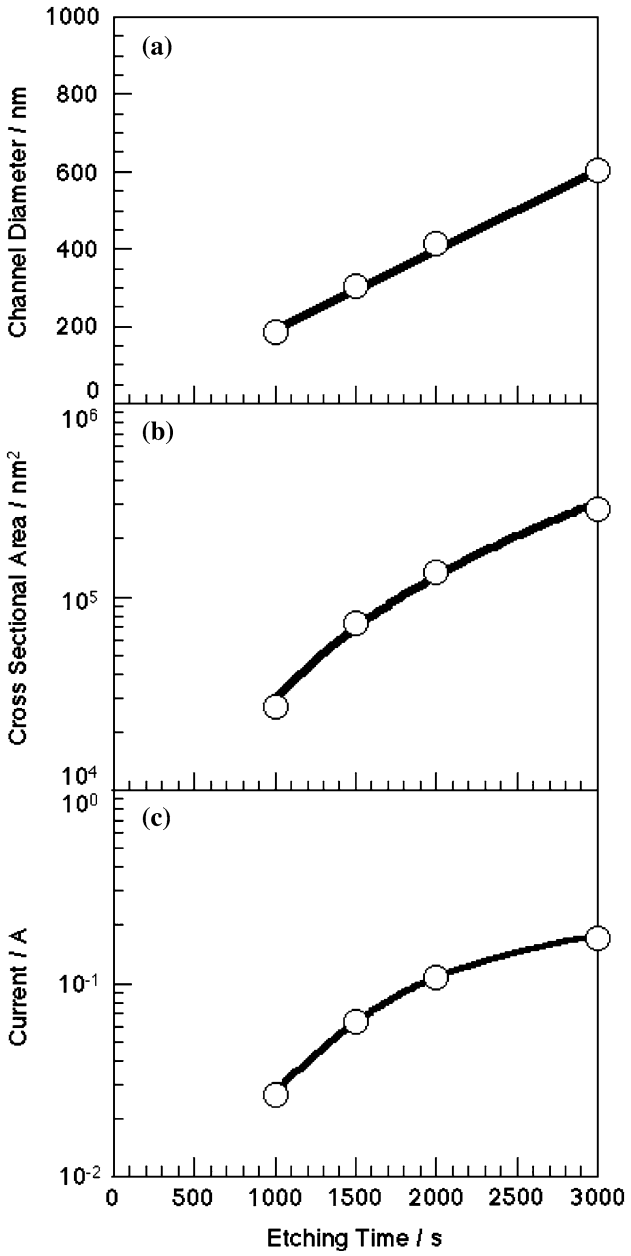

Fig. 5 Time-dependence of channel diameter (**a**), cross-sectional area of channel (**b**), and measured current (**c**), during ion-track etching of a polycarbonate film with thickness 30 μm in 6 M NaOH solution

After 1,000 s, the diameter is estimated to be around 200 nm. The channel diameter D_t (nm) at etching time t (s) can be estimated as follows.

$$D_t = 0.20 \cdot t \tag{1}$$

Here, t (s) is larger than the break-through time of 300 s. The radial etching rate is estimated to be circa 0.10 nm s^{-1}, and a channel diameter down to 60 nm could be obtained in this experimental condition. Apel et al. reported a radial etching rate of about 0.1 nm s^{-1} for heavy-ion tracks in polycarbonate films with thicknesses 10 μm [19]. Pépy et al. also reported that the radial etching rate in such films with thicknesses 20 μm was around 0.2 nm s^{-1}, respectively [21]. These data agree well with the result obtained in this study. As shown in Fig. 5b, c, the time-dependence of the cross-sectional area corresponds well to the time-dependence of measured current. The channel diameter D_t (nm) at a given current I_t (A) can be estimated as follows.

$$D_t = 1.3 \times 10^3 \cdot I_t^{0.5} \tag{2}$$

At an etching time of 1,000 s, I_t is around 2.5 × 10^{-2} A and D_t is estimated to be of the order of 200 nm.

3.2 Electrodeposition of nanowires

Figure 6 shows the effect of the cathode potential on the time-dependence of the cathodic current during Co–Cu alloy nanowire deposition in the polycarbonate template with channel length 30 μm and diameter 200 nm. The cathode potentials were fixed to −0.7, −0.9, −1.1, and −1.3 V. To determine the wire growth rate, the channel-filling time was estimated by monitoring the deposition current. When the wires reach the membrane surface, the current will increase drastically due to the formation of hemispherical caps. If the radius of a hemispherical cap increases linearly with increase in deposition time, the

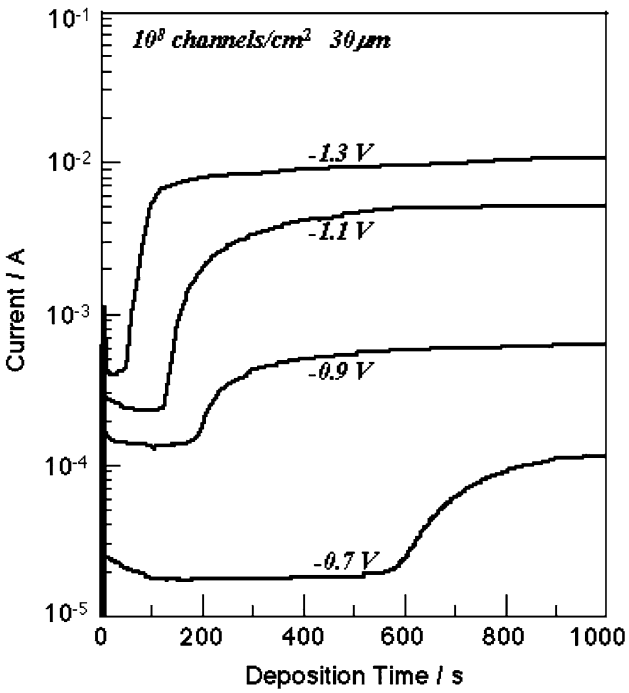

Fig. 6 Effect of cathode potential on measured current during Co–Cu alloy nanowire deposition in a polycarbonate template with channel length 30 μm and diameter 200 nm. The cathode potentials were −0.7, −0.9, −1.1, and −1.3 V

current increases in proportion to the square of deposition time because the current linearly depends on the surface area of a hemispherical cap. Deposition rates were estimated by dividing channel length by channel-filling time. At −0.7 V, this time is around 600 s and the deposition rate is estimated to be about 50 nm s^{-1}, while the filling time is close to 60 s at −1.3 V and the deposition rate is estimated to be around 500 nm s^{-1}.

Figure 7a shows a cathodic polarization curve of polycarbonate template with channel length 30 μm and diameter 200 nm. The growth rate of Co–Cu alloy nanowires electrodeposited at each cathode potential is also shown in Fig. 7b. The equilibrium potentials of Cu and Co are estimated to be around +0.05 and −0.48 V (vs.Ag/AgCl) on the basis of the Nernst equation as follows.

$$E^{eq} = E^0 + RT \cdot (nF)^{-1} \cdot \ln C_M \quad (3)$$

Here, E^0 is the standard electrode potential, and C_M denotes the concentration of metal ions (Cu^{2+} or Co^{2+}). The cathodic current occurs at the potential region close to the equilibrium potential of Cu as shown in Fig. 7a. It is well-known that Cu^{2+} ions begin to electrodeposit without an accompanying overpotential from the aqueous solution. Therefore, this cathodic current corresponds to the deposition current of Cu. With increasing cathodic current, at around 10^{-5} A, the potential significantly polarizes to the less-noble region. This phenomenon seems to be caused by the diffusion control of Cu^{2+} ions. In the potential region less-noble than the equilibrium potential of Co, the cathodic current increases again at circa −0.8 V. It is also well-known that the electrodeposition of iron-group metals such as Ni, Co, and Fe is accompanied by the overpotential [22, 23] due to the rate determining multi-step reduction mechanism [24]. Therefore, this increase in cathodic current is mainly caused by the deposition current of Co. As depicted in Fig. 7b, the potential dependence of growth rate for the nanowires corresponds well to the polarization curve for Cu and Co deposition. On the basis of the results shown in Fig. 7, the optimum deposition potentials of Cu and Co are determined to be about −0.3 and −1.0 V (vs. Ag/AgCl), that is, at potentials nobler than the diffusion control region of each metal ion. Typical deposition rates of Cu and Co were roughly 20 nm s^{-1} (at −0.3 V) and 200 nm s^{-1} (at −1.0 V).

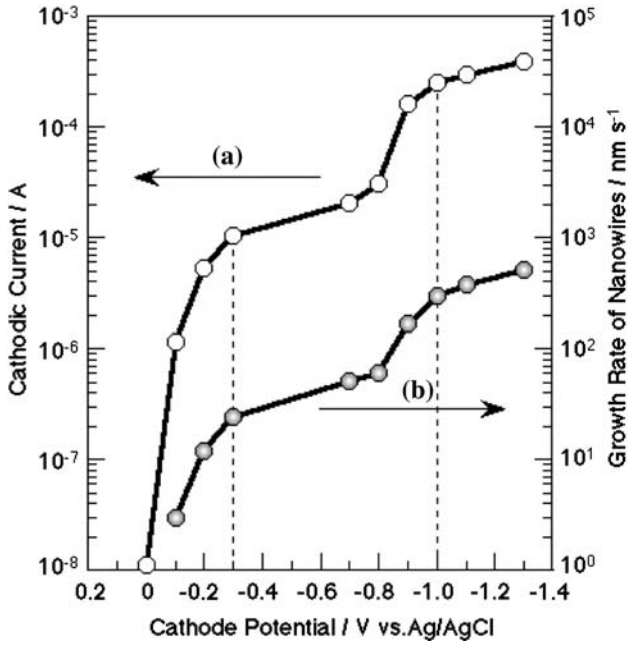

Fig. 7 Cathodic polarization (**a**) and growth rate (**b**) of Co–Cu alloy nanowires, both as a function of applied cathode potential during electrodeposition in a polycarbonate template with channel length 30 μm and diameter 200 nm

3.3 Magnetoresistance of nanowires

Figure 8 exhibits the magnetoresistive hysteresis of Co–Cu alloy nanowires electrodeposited at −1.0 V in a polycarbonate template with channel length 30 μm and diameter 200 nm. Here, θ is defined as the angle between the

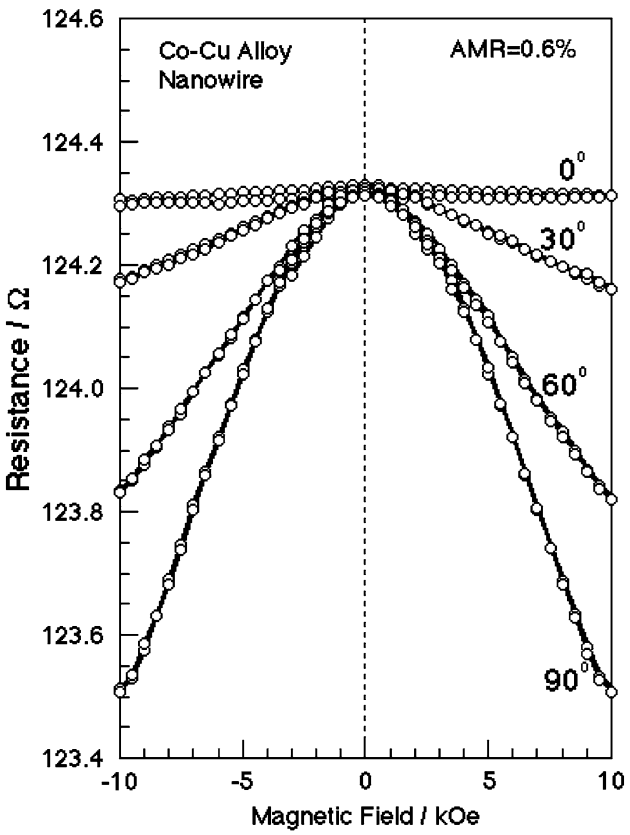

Fig. 8 Magnetoresistance of Co–Cu alloy nanowires with length 30 μm and diameter 200 nm electrodeposited into polycarbonate nanochannels

magnetic field and the nanowire axis (current direction). The MR ratio is defined by the following equation

$$\text{MR ratio}\,(\%) = 100(R_0 - R_{10})/R_{10} \quad (4)$$

Here, R_0 and R_{10} are the resistance of zero field and 10 kOe, respectively. AMR curves show the usual dependence on the direction of the applied magnetic field. In the direction parallel to the wire (0°), the effect of magnetic field on the resistance was very small and the MR ratio was almost 0, while in the direction perpendicular to the wire (90°), the MR effect was maximum. An AMR ratio of 0.6% was observed for $Co_{81}Cu_{19}$ alloy wires, which is typical of this system.

Figure 9 shows the magnetoresistive hysteresis of Co/Cu multilayered wires electrodeposited in polycarbonate film. The wire length is 30 μm and the diameter is 200 nm. The layer thickness of Co and Cu amounts to 10 nm. The structure of Co/Cu nanowires electrodeposited in polymer templates is illustrated schematically in Fig. 9. GMR strongly depends on Co and Cu layer thickness, and a maximum effect could be observed at about 10 nm [11]. Therefore, a thickness of 10 nm was realized for each layer by controlling the deposition time. The GMR curves of Co/Cu multilayered nanowires possess only a small angular dependence, and the MR ratio reaches up to 8.0%. For these samples, the saturation field seems to be around 5 kOe, which is much smaller than the field from which the AMR curves of Co–Cu alloy nanowires result. We have already reported that in porous alumina membranes Co/Cu nanowires containing 100 and 300 bi-layers showed 20 and 12% of GMR ratio [11], respectively, while the Co/Cu nanowires containing 1,500 bi-layers showed 8.0% in this study. It is not surprising that the GMR ratio of Co/Cu nanowires will decrease when increasing the number of bi-layers. For example, this GMR decrease could be caused by the enhancement of Co/Cu interfacial roughness with increasing the number of bi-layers.

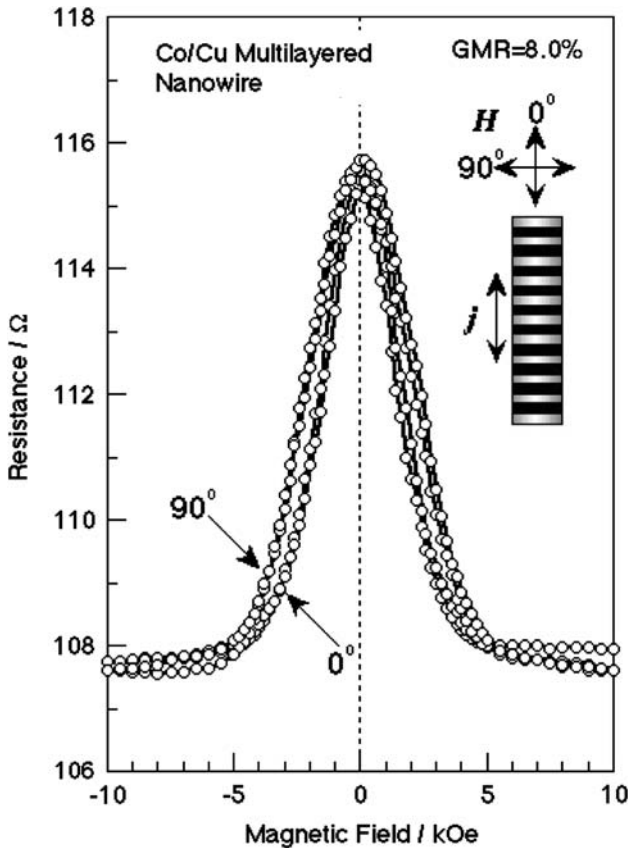

Fig. 9 Magnetoresistance of Co/Cu multilayered nanowires with length 30 μm and diameter 200 nm electrodeposited in polycarbonate nanochannels. The layer thickness of Co and Cu is 10 nm

4 Conclusion

Heavy-ion tracks in polycarbonate films were selectively etched using a 6-M aqueous solution of NaOH to produce cylindrical nanochannels. The etching rate parallel to the ion track direction was estimated to be around 50 nm s^{-1}. The channel diameters were tuned between 200 and 600 nm by varying the etching time, and the etching rate perpendicular to the ion track direction was estimated to be of the order of 0.2 nm s^{-1}. Co–Cu alloy nanowires and Co/Cu multilayered nanowires were successfully electrodeposited. The typical Cu deposition rate was about 20 nm s^{-1} at the cathode potential of −0.3 V, while the deposition rate of Co-rich alloy was circa 200 nm s^{-1} at −1.0 V. Co-rich alloy electrodeposited at −1.0 V consisted of 81%-Co and 19%-Cu. Alternating Cu- and Co-rich layers of thickness 10 nm were synthesized by pulse plating. 0.6% of AMR on Co–Cu alloy nanowires and 8.0% of GMR on Co/Cu nanowires were demonstrated for magnetic sensor applications.

Acknowledgements This work was supported in part by the European Network on Ion Track Technology (EuNITT, HPRN-CT-2000-00047), Mitutoyo Association for Science and Technology (MAST), Yazaki Memorial Foundation for Science and Technology, Research Foundation for Materials Science, Japan Society for the Promotion of Science (Grant-in-aid for Young Scientists B: No.17760581 and Grant-in-aid for Scientific Research C: No.19560734), and Nanotechnology Researchers Network Center of Japan (Japan–Sweden Young Researchers Exchange Program on Nanotechnology, 2006).

References

1. Martin CR (1991) Adv Mater 3:457
2. Whitney TM, Jiang JS, Searson PC, Chien CL (1993) Science 261:1316
3. Martin CR (1994) Science 266:1961
4. Piraux L, George JM, Despres JF, Leroy C, Ferain E, Legras R, Ounadjela K, Fert A (1994) Appl Phys Lett 65:2484

5. Blondel A, Meier JP, Doudin B, Ansermet JP (1994) Appl Phys Lett 65:3019
6. Evans PR, Yi G, Schwarzacher W (2000) Appl Phys Lett 76:481
7. Aimawlawi D, Coombs N, Moskovits M (1991) J Appl Phys 70:4421
8. Forrer P, Schlottig F, Siegenthaler H, Textor M (2000) J Appl Electrochem 30:533
9. Nielsch K, Müller F, Li AP, Gösele U (2000) Adv Mater 12:582
10. Ohgai T, Hoffer X, Gravier L, Wegrowe JE, Ansermet JP (2003) Nanotechnology 14:978
11. Ohgai T, Hoffer X, Fabian A, Gravier L, Ansermet JP (2003) J Mater Chem 13:2530
12. Ohgai T, Gravier L, Hoffer X, Lindeberg M, Hjort K, Spohr R, Ansermet JP (2003) J Phys D: Appl Phys 36:3109
13. Dobrev D, Vetter J, Angert N, Neumann R (1999) Appl Phys A: Mater Sci Process 69:233
14. Siwy Z, Dobrev D, Neumann R, Trautmann C, Voss K (2003) Appl Phys A: Mater Sci Process 76:781
15. Siwy Z, Apel P, Baur D, Dobrev D, Korchev YE, Neumann R, Spohr R, Trautmann C, Voss K (2003) Surf Sci 532–535:1061
16. Enculescu I, Siwy Z, Dobrev D, Trautmann C, Toimil Molares ME, Neumann R, Hjort K, Westerberg L, Spohr R (2003) Appl Phys A: Mater Sci Process 77:751
17. Chtanko N, Toimil Molares ME, Cornelius T, Dobrev D, Neumann R (2004) J Phys Chem B 108:9950
18. Dobrev D, Baur D, Neumann R (2005) Appl Phys A: Mater Sci Process 80:451
19. Apel P, Akimenko A, Blonskaya I, Cornelius T, Neumann R, Schwartz K, Sphor R, Trautmann C (2006) Nucl Instr Methods B 245:284
20. Chtanko N, Toimil Molares ME, Cornelius T, Dobrev D, Neumann R (2005) Nucl Instr Methods B 236:103
21. Pépy G, Boesecke P, Kuklin A, Manceau E, Schiedt B, Siwy Z, Toulemonde M, Trautmann C (2007) J Appl Cryst 40:388
22. Tsuru T, Kobayashi S, Akiyama T, Fukushima H, Gogia SK, Kammel R (1997) J Appl Electrochem 27:209
23. Ohgai T, Enculescu I, Zet C, Westerberg L, Hjort K, Spohr R, Neumann R (2006) J Appl Electrochem 36:1157
24. Bockris JO'M, Kita H (1961) J Electrochem Soc 108:676